U.S. DEPARTMENT OF ENERGY | Office of Science

DOE/SC-ARM-TR-234

Atmospheric Emitted Radiance Interferometer Optimal Estimation (AERIoe) Value-Added Product Report

LD Riihimaki
T Shippert
DD Turner

November 2019

ARM

DISCLAIMER

DOE/SC-ARM-TR-234

Atmospheric Emitted Radiance Interferometer Optimal Estimation (AERIoe) Value-Added Product Report

LD Riihimaki, Cooperative Institute for Research in Environmental Sciences
T Shippert, Pacific Northwest National Laboratory
DD Turner, National Oceanic and Atmospheric Administration

November 2019

Work supported by the U.S. Department of Energy,
Office of Science, Office of Biological and Environmental Research

Executive Summary

The Atmospheric Emitted Radiance Interferometer (AERI) Optimal Estimation (AERIoe) algorithm (Turner and Löhnert 2014, Turner and Blumberg 2019) retrieves profiles of temperature and water vapor mixing ratio, together with cloud properties for a single-layer cloud (i.e., liquid water path [LWP], effective radius), from AERI-observed infrared radiance spectrum and other measurements. The data can be used to characterize the evolution of the planetary boundary layer and boundary-layer clouds.

Acknowledgments

Many thanks to Krista Gaustad for providing liquid water path plots and helping facilitate implementation of operational retrievals.

Acronyms and Abbreviations

AER	Atmospheric and Environmental Research
AERI	atmospheric emitted radiance interferometer
AERIoe	Atmospheric Emitted Radiance Interferometer Optimal Estimation VAP
AERIPROF	Atmospheric Emitted Radiance Interferometer Profiles of Water Vapor and Temperature VAP
AMF	ARM Mobile Facility
ARM	Atmospheric Radiation Measurement
CAPE	convectively available potential energy
CIN	convective inhibition
CLDTYPE	Cloud Type VAP
DISORT	Discrete Ordinate Radiative Transfer Program for a Multi-Layered Plane-Parallel (Medium)
GoAmazon	Green Ocean Amazon 2014/15 field campaign
IDL	Interactive Data Language
IR	infrared
KAZR	Ka-band ARM Zenith Pointing Radar
LBLRTM	Line-By-Line Radiative Transfer Model
LWP	liquid water path
MET	surface meteorological instrumentation
MIXCRA	mixed-phase cloud property retrieval algorithm
MonoRTM	Monochromatic Radiative Transfer Model
MPL	micropulse lidar
MWR	microwave radiometer
MWR3C	3-channel microwave radiometer
MWRLOS	2-channel microwave radiometer
MWRRET	Microwave Radiometer Retrievals VAP
NWP	numerical weather prediction
PECAN	Plains Elevated Convection at Night campaign
QC	quality control
RAP	rapid refresh model
RHUBC-2	second Radiative Heating in Underexplored Bands Campaign
RMS	root mean square
SGP	Southern Great Plains
TCCON	Total Carbon Column Observing Network
TSI	total sky imager
UTC	Coordinated Universal Time
VAP	value-added product

Contents

Figures

Tables

1.0 Introduction

The AERIoe algorithm (Turner and Löhnert 2014, Turner and Blumberg 2019) retrieves boundary-layer profiles of temperature and water vapor mixing ratio, together with cloud properties for a single-layer cloud (i.e., LWP, effective radius), from AERI-observed infrared radiance spectra and other measurements. The current AERIoe Value-Added Product (VAP) uses version 2.8 of David Turner's code, which uses additional inputs to constrain the retrieval including surface meteorology, microwave radiometer brightness temperatures at any number of frequencies (the U.S. Department of Energy Atmospheric Radiation Measurement [ARM] user facility typically used observations at 23.8 and 30.0 GHz), and Rapid Refresh numerical weather prediction model output. The method is a physical-iterative retrieval that uses the optimal estimation framework (Rodgers 2000), so a full error covariance of the solution and the information content (in the form of degrees of freedom for signal) is provided for each retrieval.

AERIoe offers a number of improvements over the Atmospheric Emitted Radiance Interferometer Profiles of Water Vapor and Temperature (AERIPROF) VAP (Feltz et al. 2003) that is ARM's current data product for thermodynamic profiles from the AERI. First, AERIoe is not limited to clear-sky cases, and is able to retrieve thermodynamic profiles in cloudy conditions by also retrieving the cloud properties simultaneously (Turner and Löhnert 2014). The algorithm, when both AERI and microwave radiometer (MWR) data are used as input, retrieves the LWP of clouds over the entire range of LWP with less than 20% uncertainty (Turner 2007), including those less than 60 g m^{-2}, a critical need for shallow cumulus measurements. Second, the use of a weighting factor in the optimal estimation methodology is less sensitive to having a good initial guess to implement in the forward model (Turner and Löhnert 2014). This gives higher accuracy, and also allows the VAP to be run at sites beyond ARM's Southern Great Plains (SGP) atmospheric observatory, something that has not been done with AERIPROF. Finally, the optimal estimation methodology produces uncertainties, including a full error covariance matrix, and fields related to the vertical distribution of the information content along with the thermodynamic profiles.

2.0 Input Data

The primary input to this code is AERI downwelling infrared radiance spectra, from the AERI Noise Filter datastream (Turner et al. 2006). Additional AERI quality information is taken from aeriengineer and aerisum files.

The AERI measures downwelling spectral infrared radiance in the wavelength range 3.3-19.2 microns (520-3020 cm^{-1} wavenumbers). This is the terrestrial radiation (LW) wavelength range, so it provides a great deal of information about temperature and humidity profiles in the boundary layer, and liquid water for liquid water paths less than 60 g m^{-2} or so (Turner 2007). Details of the AERI, including how it is calibrated, are provided by Knuteson et al. (2004 a,b), and in the ARM AERI Instrument Handbook (https://www.arm.gov/publications/tech_reports/handbooks/aeri_handbook.pdf).

In addition to infrared (IR) spectra from the AERI, the 23.8 and 30 GHz channels of the microwave radiometer are used to help better constrain the precipitable water vapor and liquid

water path for liquid water paths above about 60 g m^{-2}. The ARM facility has deployed different MWRs at different sites, and the AERIoe algorithm can use MWR observations at any frequency. At the SGP Central Facility, we are currently using the 2-channel microwave radiometer (MWRLOS), and at the SGP extended facilities we are using the 3-channel microwave radiometers (MWR3C).

Surface temperature and relative humidity are taken from the 2 m surface meteorological instrumentation (MET) data available at nearly all ARM sites and facilities.

Cloud base heights come either from the ceilometer when available (e.g., SGP Central Facility) or from alternative lidar sources such as the Doppler lidar at SGP boundary facilities.

Finally, we use averaged model output from the rapid refresh (RAP) model (Benjamin et al. 2016) from 4 km to 20 km to constrain the thermodynamic profiles of the upper atmosphere since the AERI has very little information content above the boundary layer.

AERIoe is able to include other inputs, such as Raman lidar thermodynamic profiles, into its observation vector as part of the retrieval (Turner and Blumberg 2019). Currently, these other observations are not being used operationally by ARM in this version, but may be included in the future. Note that the AERIoe algorithm can be run at any of the ARM sites that contain an AERI (e.g., Turner and Blumberg 2019 analyzed data from the ARM sites at Oliktok Point, Alaska and the ARM Mobile Facility [AMF] deployment to the Green Ocean Amazon 2014/15 [GoAmazon] campaign in Brazil), but currently only the SGP data are being processed by this algorithm.

3.0 Output Data

The VAP output files contain primary scientific variables, random uncertainty estimates as output by the algorithm, some calculated thermodynamic profile parameters (relative humidity, potential temperature, equivalent potential temperature, dew point temperature), variables related to the information content of the observations (e.g., degrees of freedom for signal, true vertical resolution of the retrieved profiles, and Shannon information content), and a number of diagnostic variables that describe the state of the retrieval. In the current version, the primary scientific output variables are temperature, humidity profiles, liquid water path, liquid cloud effective radius, and their uncertainties as listed in Table 1.

In general, the files have been left in a similar format to the output from Dr. Turner's native code, with minor adjustments to meet ARM standards. We have left in some empty variables that are currently not retrieved (i.e., are disabled in this implementation in the ARM data system due to their research nature) but may be in the future, such as ice cloud properties (ice cloud optical depth, ice effective radius) and trace gas concentrations (CO_2, CH_4, N_2O).

Table 1. Table of primary scientific variables currently output by the retrieval algorithm.

Variable	Description	Uncertainty variable
temperature	Temperature profile (degC)	sigma_temperature
waterVapor	Water vapor mixing ratio profiles (g kg^{-1})	sigma_waterVapor
lwp	Liquid water path (g m^{-2})	sigma_lwp
lReff	Liquid water effective radius (microns)	sigma_lReff

4.0 Algorithm Overview

The AERIoe algorithm is described in detail elsewhere (Turner and Löhnert 2014, Turner and Blumberg 2019), but will be summarized here. The algorithm uses an optimal estimation approach (Rodgers 2000) to simultaneously retrieve temperature and water vapor profiles, as well as cloud LWP and effective radius for liquid clouds, from observational data including AERI radiances in the wavenumber bands listed in Table 2. Version 1 of the algorithm (Turner and Löhnert, 2014) used only AERI radiances and cloud base height as input, but version 2 of the algorithm (Turner and Blumberg, 2019) incorporates various other observational inputs including surface MET observations, partial profiles from NWP model output, and microwave radiometer brightness temperatures. Version 2.8 is used in the VAP currently and incorporates the inputs described in Section 2 of this technical report.

This is a physical-iterative retrieval method. The retrieval of thermodynamic profiles from spectral radiance observations is an ill-posed problem, and thus constraints need to be included in the retrieval algorithm to provide physically plausible results. Here, we use a climatology derived from radiosonde profiles collected at the measurement site as our prior information. At the SGP site, where radiosondes have been launched for nearly 30 years, monthly climatology “a priori” files have been computed, wherein data from three months centered upon the month desired are used to compute the level-to-level covariance in the a priori. For example, to compute the a priori input file for July, all of the radiosonde data launched at the SGP Central Facility between 2000 and 2015 from June, July, and August were used in the calculation of the a priori. Over 2000 radiosondes have been used to compute the a priori for each month at the SGP.

As the method uses an optimal estimation framework, a full error covariance matrix of each solution is included in the output file. The 1-sigma uncertainty of each retrieved variable, which is derived from the error covariance matrix, is included for each scientific field and is named "sigma_X", where "X" is the name of the scientific field (e.g., 'temperature').

Table 2. Wavenumber bands used in retrieval, based on Table 1 of Turner and Blumberg (2019).

Wavenumber band (cm^{-1})	Primary sensitivity
538-588	Water vapor
612-618	Temperature
624-660	Temperature
674-722	Temperature
828-835	Clouds
843-848	Clouds
860.1-864	Clouds
872.2-877.5	Clouds
898.2-905.4	Clouds

4.1 Prior Values

Prior temperature and humidity profiles come from monthly climatologies created from radiosonde data. These will be fixed for a given site. All times of day and cloud conditions are averaged together to form the climatologies. The vertical resolution of the prior profiles is also the same as the vertical grid output by the retrieval. The prior includes covariances between the variable at a given height and other heights in the profile. The a priori computed at the SGP Central Facility is also used when processing data from the SGP extended facility sites.

The assumed a priori cloud properties are currently set to values of LWP= 0 ±50 g m^{-2}, and Reff = 8±4 μm. There is assumed to be no correlation between cloud properties and thermodynamic profiles in the prior.

4.2 Assumed Inputs

Cloud base height is taken from ceilometer measurements for a 20-minute interval. If no cloud base is found, this is expanded to a 180-minute interval. Finally, if no measured cloud base height is found, a default value of 2 km is used. Cloud base height is not adjusted by the retrieval in this version, and any uncertainty in cloud base height is not included in the uncertainty estimates.

Additionally, height independent values of CO_2, CH_4, and N_2O concentrations are set in the config file. Total column CO_2 concentration is estimated from a statistical model fit to Mauna Loa data that accounts for both the general increase in CO_2 over time and the annual cycle. Currently, constant values of 1.793±0.0538 ppm and 0.310±0.0093 ppm are used for CH_4 and N_2O respectively. These are based on measurements from the Total Carbon Column Observing Network (TCCON) at SGP. These are left constant and not simultaneously retrieved in the operational version, though there is the potential to also retrieve these values in the future. Due to the location of the absorption bands of CH_4 and N_2O, and the spectral regions used in the retrieval (Table 2), there is virtually no sensitivity of the retrieved profiles to these assumed concentrations.

4.3 Forward Model

The Line-By-Line Radiative Transfer Model (LBLRTM; Clough and Iacono, 1995) from AER (https://rtweb.aer.com/lblrtm_frame.html) is used to model the infrared radiances. We are currently using version 12.1. Version 12.8 is also now currently available but the differences between versions 12.1 and 12.8 in the spectral regions being used for this application are small, so we have chosen to continue using 12.1. The LBLRTM has been improved and validated extensively using data from many of the ARM sites (e.g., Mlawer and Turner 2016, and is able to simulate AERI observations well.

The Monochromatic Radiative Transfer Model (MonoRTM; Clough et al. 2005) from Atmospheric and Environmental Research (AER) (https://rtweb.aer.com/monortm_frame.html) is used as the forward model for the microwave frequencies used in the retrieval. We are currently using model version 5.2. This model has also been improved and extensively validated using ARM data (e.g., Payne et al. 2011, Turner et al. 2016).

The retrieval is currently run for AERI wavenumber bands given in Table 2. These are the same wavenumber bands used for the AERIPROF retrieval except the 1250-1350 cm^{-1} band is used by AERIPROF but not in AERIoe. This is because this wavenumber band is strongly influenced by scattering from cloud particles (Turner and Löhnert 2014), and only absorption (not scattering) is currently implemented in the forward model used in AERIoe.

5.0 Interpretation of the Data and Quality Control

There are several important things to note when interpreting the AERIoe data.

First, the information content in the AERI observations, which is in the degrees of freedom for signal ("dfs") field, on the thermodynamic profiles is primarily concentrated in the lowest 3 km or up to cloud base; the retrieved data should not be used above that level (or used with caution).

Second, the true vertical resolution is not the same as the vertical height grid used in the retrievals. The weighting functions for downwelling radiance observations often peak near the surface and thus the vertical resolution of the retrieved profiles decreases quickly with height. The actual vertical resolution of the retrieval is estimated from the averaging kernel computed by the retrieval algorithm, and are stored in the variables “vres_temperature” and “vres_watervapor” in the output file. Examples of the vertical resolution are shown in Turner and Löhnert (2014).

Third, the retrieval should only be used when the run converges. There is an overall "qc_flag" field; however, the logic that sets this flag is still being developed and should not be used at this time. Instead, a more straightforward way to determine when the data can be used is to consider all retrievals that have a value for "converged_flag" greater than 0 and less than 9 as valid. Furthermore, there are two root mean square (RMS) fields that compare the observations with the forward calculation using the final retrieved fields (“rmsr” and “rmsa”), where the former compares only the radiance observations from the AERI and MWR whereas the latter compares the entire observation vector (which could contain surface MET and NWP data as well) with the forward calculation. Generally, only samples where the “rmsr” field is less than 5 should be used, but retrievals with values larger than this threshold may still contain useful information.

Finally, uncertainty values are given for each of the primary scientific variables by the optimal estimation algorithm. Please note, however, that these only include the correlated error propagated through from the prior, the random error in the observations, and the sensitivity of the forward model. There are several known conditions that cause systematic errors in the current retrieval. Ice clouds can cause biases in the liquid water path retrievals, if ice water contents are retrieved as liquid water. Additionally, due to the decrease in the vertical resolution with altitude, the AERIoe may not be able to resolve elevated inversions or localized gradients away from the surface. For example, the AERIoe-retrieved profiles may not resolve the inversion layer at the top of the convective boundary layer because the actual vertical resolution at that altitude may be 1 km or more. However, that information is still in the retrieved profile, as integrated values such as mixed-layer Convectively Available Potential Energy (CAPE) and Convective Inhibition (CIN) computed from AERIoe-retrieved profiles compare reasonably well with values computed from co-located radiosonde data (Blumberg et al. 2017).

More details on the evaluation of the retrieval can be found in Turner and Blumberg (2019) and users are encouraged to read this reference before using the data.

6.0 Examples

The primary scientific variables from the AERIoe VAP are the cloud liquid water path and droplet effective radius, and boundary-layer thermodynamic profiles. We show examples of these variables here to show the strengths of the new data set.

6.1 Liquid Water Path Retrievals

Figure 1 shows the liquid water path retrieved from three different instruments and algorithms on a day with partially cloudy shallow cumulus clouds (see supporting data in Figures 2 and 3 to describe cloud conditions). The AERIoe retrieval is particularly useful for cases such as these with clouds with small liquid water paths (here ~70 g/m^2 and less). The AERIoe VAP (Figure 1, blue line) shows clear spikes in LWP between about 17:00 and 23:59 UTC consistent with when active sensors (Figure 2) and total sky imager (TSI; Figure 3) show liquid clouds. The retrievals from the 2-channel (green) or 3-channel (red) microwave radiometers often miss these spikes. Additionally, when no cloud is overhead, the AERIoe algorithm gives a LWP retrieval of zero, but both microwave radiometer retrievals show biases. The Microwave Radiometer Retrievals (MWRRET) algorithm (Turner et al. 2007) applied to the 2-channel MWR (green line) does a reasonable job at removing the larger biases but significantly more noise can be seen in the data and the measurements miss most of the shallow cumulus clouds due to insufficient sensitivity at 23 and 30 GHz to low LWP. The 3-channel MWR retrieval (red line) does not include bias corrections currently, so while the more sensitive 89 GHz channel sometimes catches the low-LWP clouds, keeping that channel bias-corrected is a significant challenge.

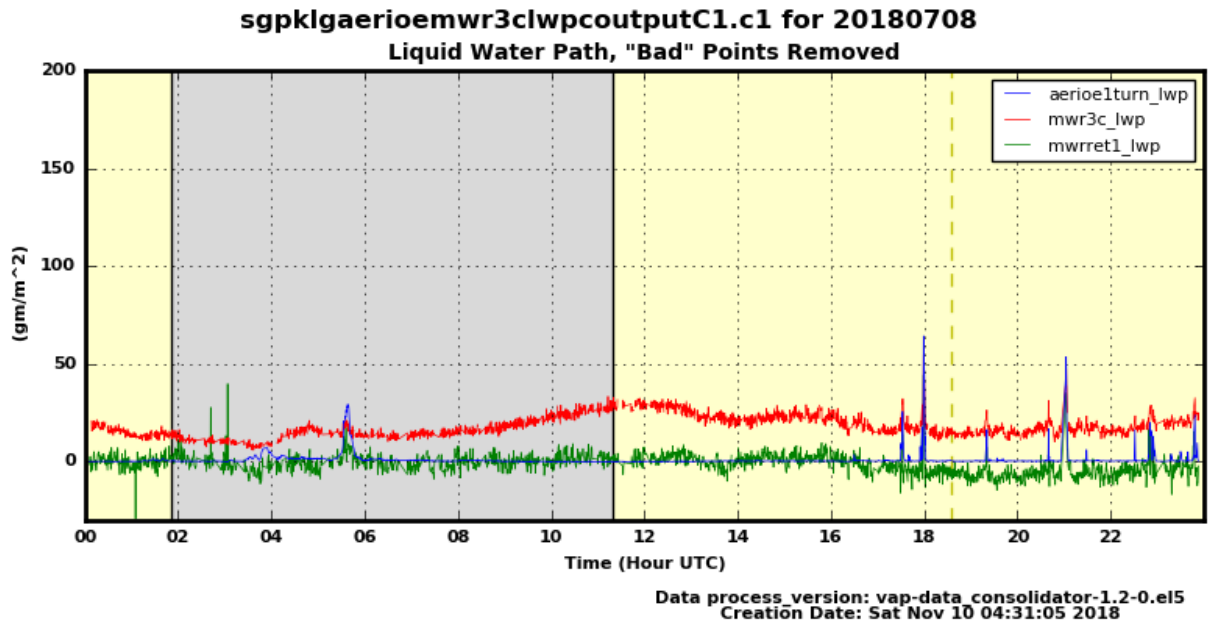

Figure 1. Example liquid water path retrievals from the AERIoe VAP (blue), the 3-channel microwave radiometer (red), and the MWRRET retrieval from the 2-channel microwave radiometer (green) from the SGP site on July 8, 2018. This day has scattered shallow cumulus clouds as confirmed in Figures 2 and 3.

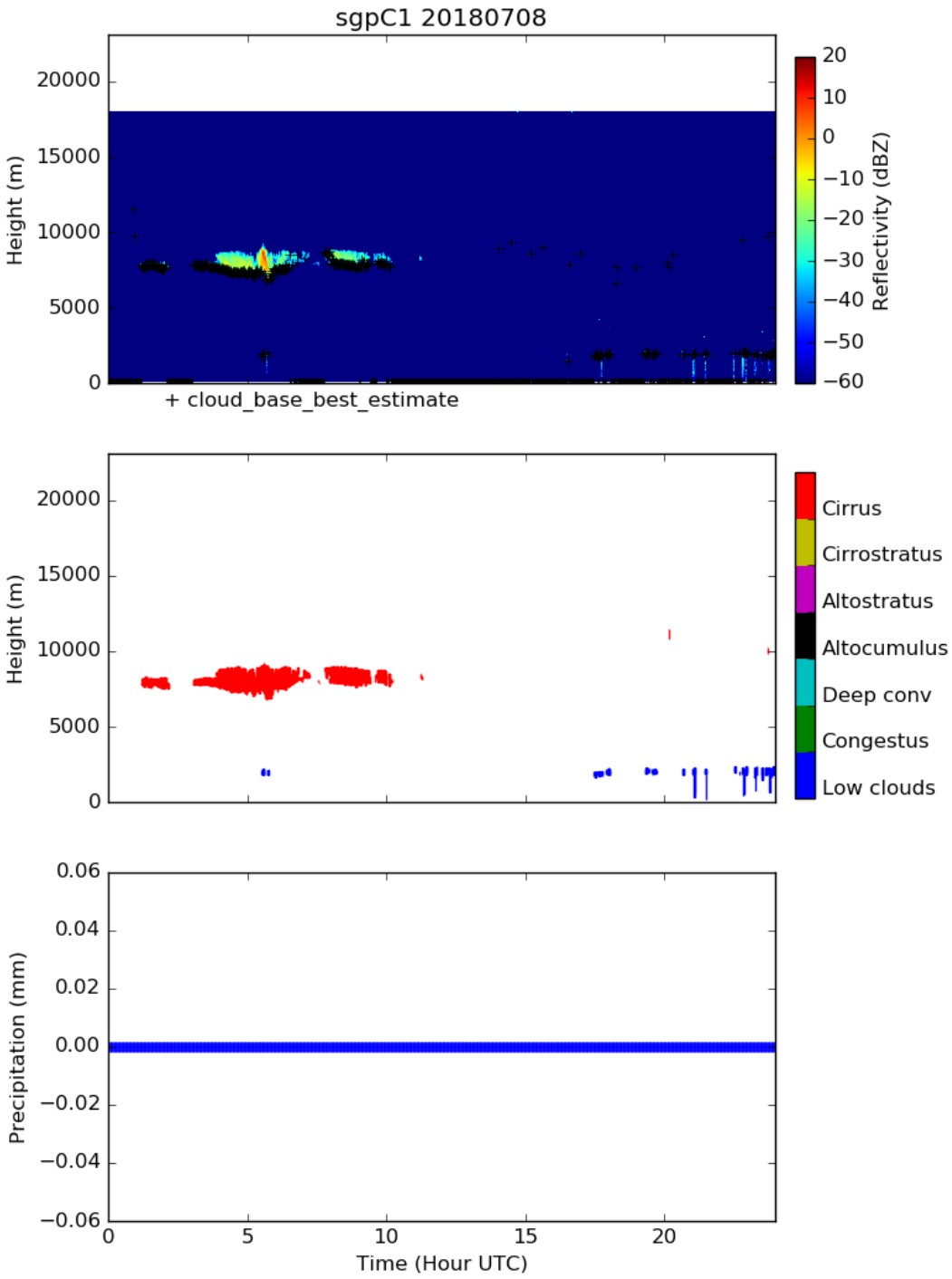

Figure 2. Ka-band ARM Zenith Pointing Radar (KAZR) radar reflectivity (top panel) **with ceilometer lowest cloud base height overlaid with black +s**, identified cloud types from the Cloud Type (CLDTYPE) VAP (Lim et al. 2019, https://www.arm.gov/publications/tech_reports/doe-sc-arm-tr-200.pdf) using KAZR and micropulse lidar (MPL) cloud boundaries (middle panel), and precipitation measurements (bottom panel) show July 8, 2018 at SGP is a day with scattered shallow cumulus between 17:00 and 23:59 UTC.

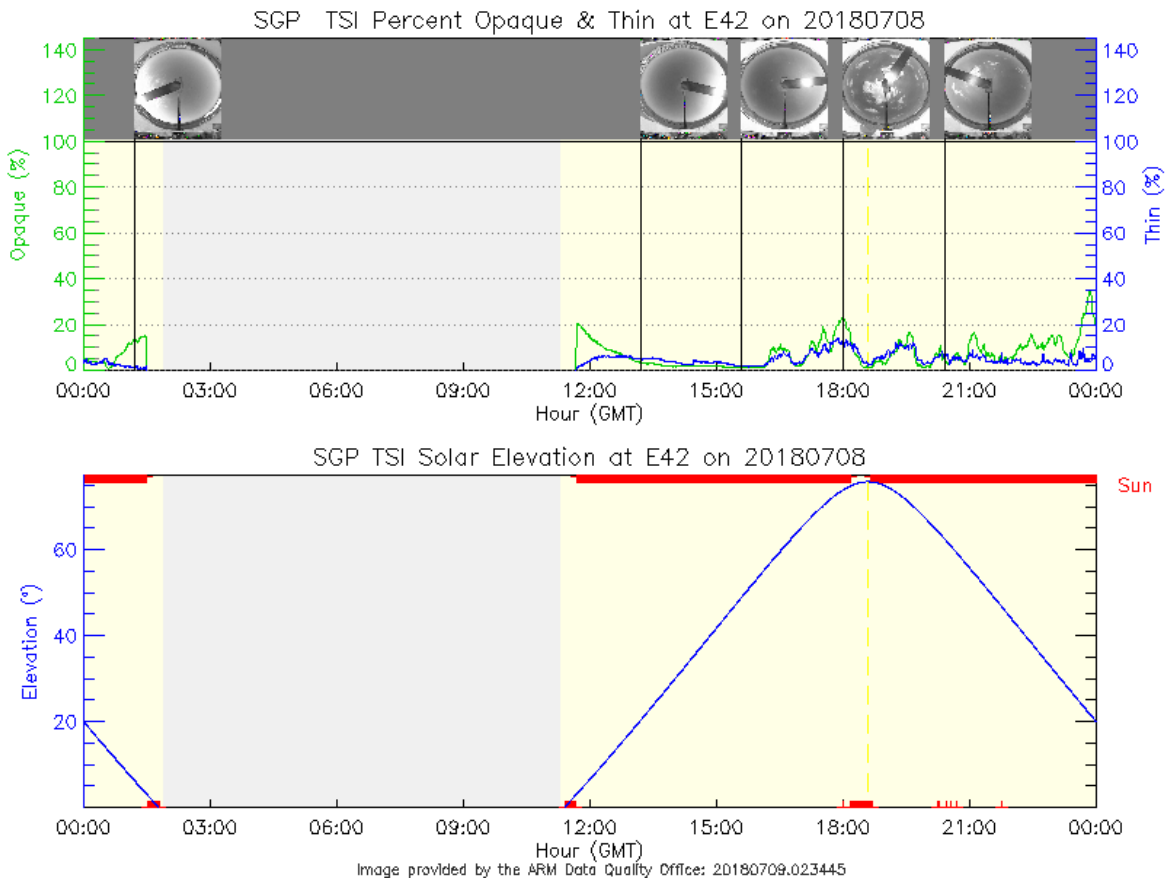

Figure 3. TSI opaque (green line top panel) and optically thin (blue line top panel) cloud fraction on July 8, 2018 at SGP. Partially cloudy skies are seen between around 17:00 and 23:59 UTC with TSI thumbnail images showing shallow cumulus clouds during this period. Bottom panel shows when the solar elevation is sufficiently high for good TSI retrievals.

6.2 Boundary-Layer Thermodynamic Profile Retrievals

Sample thermodynamic retrievals from the AERIoe retrieval are shown in Figure 4 for the same day (July 8, 2018) at SGP. One of the major advantages of the AERIoe retrieval is the high temporal resolution of the thermodynamic profile retrievals in the boundary layer. The VAP is run here at the native resolution of the AERI, or approximately 20 s frequency. The diurnal heating of the boundary layer can be seen in the temperature retrieval (Figure 4, top panel), along with a decrease in humidity in the afternoon once clouds begin to form.

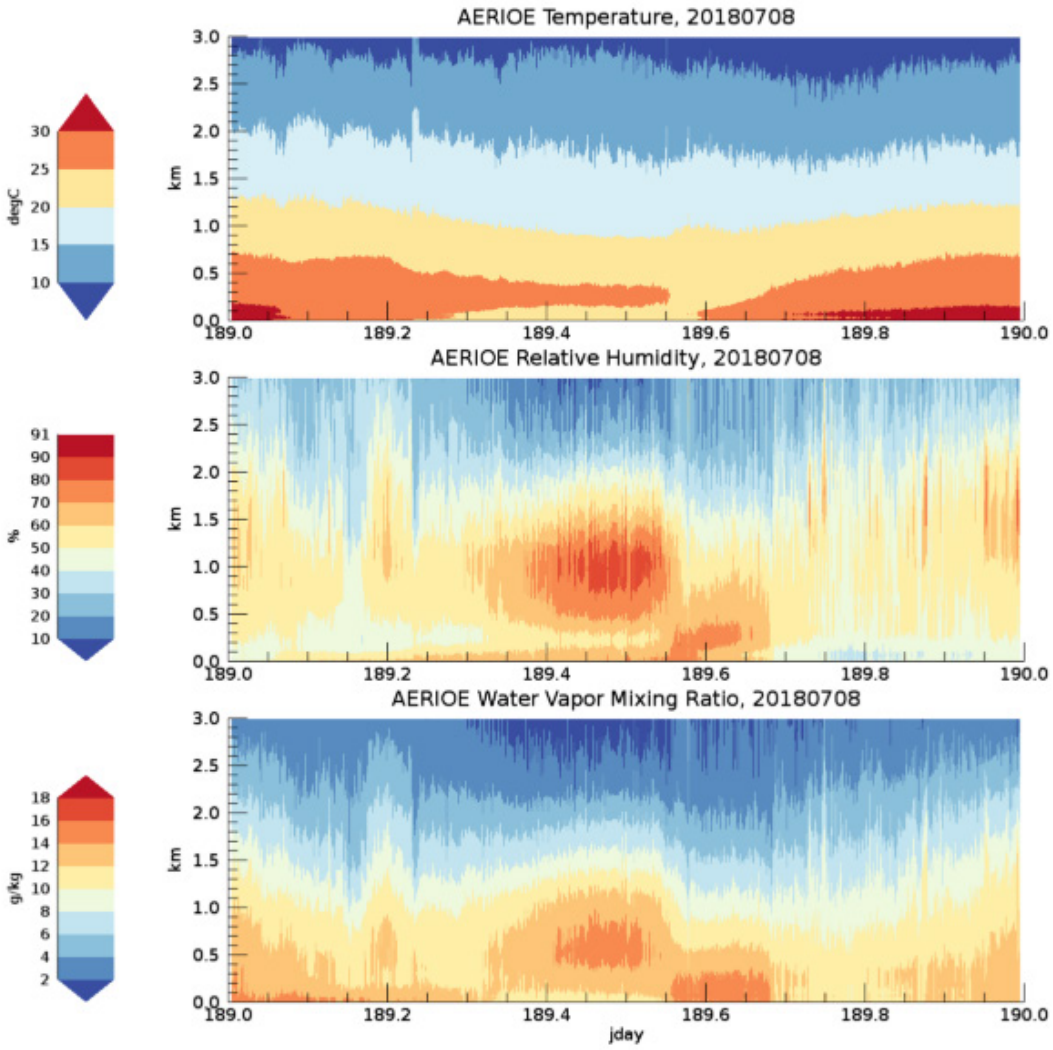

Figure 4. Boundary-layer thermodynamic profile retrievals from AERIoe at the SGP site on July 8, 2018. Temperature (top panel), relative humidity (middle panel), and water vapor mixing ratio (bottom panel) are shown. Note that the algorithm retrieves temperature and water vapor mixing ratio, and that the RH field is derived from the retrieved fields. The temporal resolution is high (approximately 20 s resolution) but the vertical resolution is fairly coarse, decreasing with range above the surface.

Comparison between radiosonde and AERIoe profile retrievals in the boundary layer shows that the AERIoe algorithm captures the overall profile quite well (e.g., Figure 5 showing an early morning profile), but can miss details that require high-resolution information, such as the humidity change at the top of the boundary layer in late afternoon (Figure 6) due to the vertical resolution of the retrieved profiles.

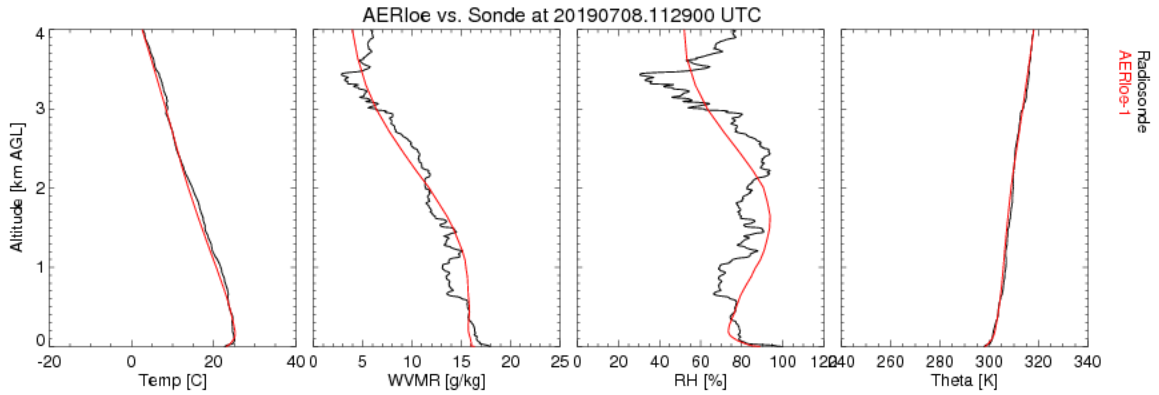

Figure 5. Sample radiosonde (black) and AERIoe-retrieved (red) boundary-layer profiles of temperature (left), water vapor mixing ratio (second from left), relative humidity (second from right), and potential temperature (right). Profiles are shown at 11:29 UTC, or 6:26 am local time. Temperature and water vapor profiles agree quite well within the coarse vertical resolution of the AERIoe retrieval.

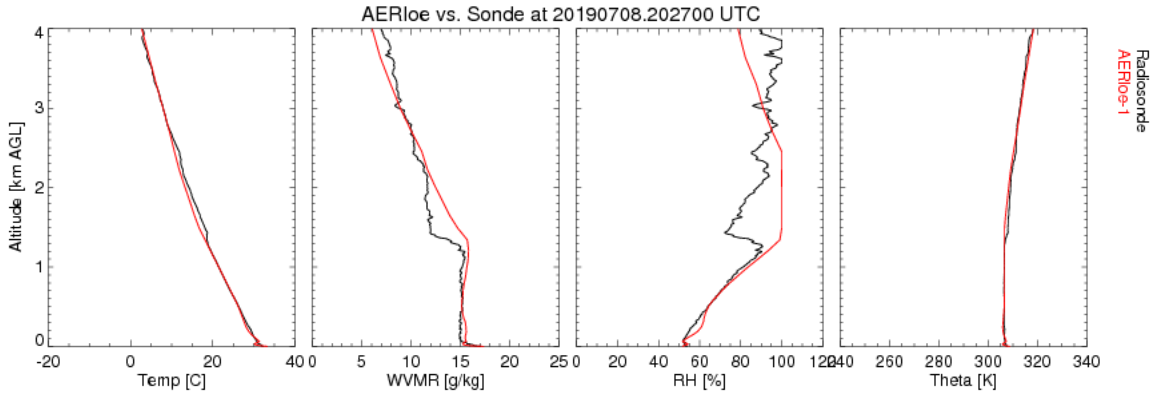

Figure 6. Same as Figure 5, but for a profile in the late afternoon, 20:27 UTC, 3:27 pm local time. Note that the AERIoe retrieval cannot capture the sharp gradient in water vapor at the top of the boundary layer due to insufficient resolution/information content, but still captures the average profile well.

Several studies have used AERIoe retrievals to improve our understanding of atmospheric phenomena. Generally speaking, these studies take advantage of the high temporal resolution of the retrievals, and the limitation of the coarse vertical resolution can be accounted for by using the data where there is information content (i.e., by considering the uncertainty information and vertical resolution fields that are provided with the output). Here are some examples:

- Toms et al. (2017) used the high temporal resolution of the AERIoe product, together with a collocated Doppler lidar, to get horizontal winds, to look at the properties of convectively generated gravity waves/undular bores that passed over the instrument site. In particular, they demonstrated that the uncertainties in the AERIoe and Doppler lidar observations were small enough that ducting layers in the lower troposphere could be identified robustly. Haghi et al. (2019) argue that a network of thermodynamic profilers such as the AERI using this algorithm are required if the community is to really understand these types of gravity waves and improve their impacts on weather forecasts.

- How the boundary layer evolves from a preconvective to convective environment is one of the outstanding scientific questions facing the severe weather community. Several studies have used AERIoe retrievals to gain insight into this evolution. One such example (Grasmick et al. 2018) looked at how the boundary layer evolved during the passage of a mesoscale convective storm, and in particular how this storm impacted the evolution of the stable boundary layer.
- Assimilating AERIoe thermodynamic profiles provides a unique opportunity to improve a mesoscale analysis, and hence improve a weather forecast. Hu et al. (2019) assimilated AERIoe and Doppler lidar profiles from the Plains Elevated Convection at Night (PECAN) campaign, which was supported by ARM (Geerts et al. 2017), to greatly improve the forecast of an EF3 tornado. Coniglio et al. (2019) assimilated AERIoe and Doppler lidar data for 12 isolated supercell storms, demonstrating that the assimilation of these advanced data sets improved the forecasts in 11 of those storms.
- Accurate thermodynamic profiles are needed to evaluate and improve radiative transfer models. During the second Radiative Heating in Underexplored Bands Campaign (RHUBC-2), the AERIoe retrievals were used to improve the temperature profiles used in the lowest 1 km of the boundary layer, which was required before the spectroscopy in the far-infrared portion of the spectrum could be evaluated and improved (Mlawer et al. 2019).
- The high temporal resolution of the AERIoe thermodynamic retrievals was used to evaluate how the boundary layer evolved during the 2017 solar eclipse (Turner et al. 2018). In particular, during that "rapid sunset/rapid sunrise" event, the AERIoe data showed that a shallow (less than 200 m) stable boundary layer developed, which contributed to the development of a low-level-jet-like wind feature.
- AERIoe-retrieved cloud properties are also being used in the development and evaluation of new subgrid-scale schemes used in numerical weather prediction models (Angevine et al. 2018).

7.0 Needs for Future Development

The current version of the AERIoe algorithm that is implemented in the ARM VAP is version 2.8. Since the ARM VAP was implemented, Dr. Turner has made additional improvements and is currently running version 2.11 of AERIoe, with minor improvements over 2.8.

In addition, several planned improvements to AERIoe in the future include updating the code to:

- Perform the retrieval on two time-scales: one for retrieving thermodynamic profiles and one for cloud property retrievals. The assumption is that the thermodynamic profiles do not need to be retrieved as often as cloud properties, and therefore that separating the retrieval into the two time-scales (the frequency of the two determined by the input parameter file) will improve the speed of the algorithm. This should allow for more focused development for cloud retrievals versus thermodynamic profiles.
- The inclusion of a first-order treatment for scattering into the forward radiative transfer model. This will help improve cloud property retrievals, particularly of ice clouds, and help to better distinguish liquid and ice clouds in the liquid and water path retrievals. The goal is to have the same accuracy at cloud property retrievals as the mixed-phase cloud property retrieval algorithm (MIXCRA; Turner 2005), which uses a Discrete Ordinate Radiative Transfer Program for a Multi-Layered Plane-Parallel (Medium) (DISORT) as the radiative transfer algorithm. (DISORT could be used within AERIoe, but that would make the retrieval about three orders of magnitude more computationally expensive.)

- Port the code from the Interactive Data Language (IDL) to the Python programming language. This work, already underway, would enable the algorithm to be run more easily on cluster-based, high-performance computing systems as the port would eliminate the need for each node to have access to an IDL license.

Lastly, we plan on implementing the AERIoe at all ARM sites that include an AERI. An important part of this work will be the development of a priori data sets at each location to constrain the retrieval.

ARM will continue to work with Dr. Turner on incorporating new versions of the code in the future as these developments become available and meet the needs of ARM's priorities.

8.0 References

Angevine, WM, JB Olson, J Kenyon, WI Gustafson Jr., S Endo, K Suselj, and DD Turner. 2018."Shallow cumulus in WRF parameterizations evaluated against LASSO large-eddy simulation." *Monthly Weather Review* 146(12): 4303–4322, https://doi.org/10.1175/MWR-D-18-0115.1

Benjamin, SG, SS Weygandt, JM Brown, M Hu, CR Alexander, TG Smirnova, JB Olson, EP James, DC Dowell, GA Grell, H Lin, SE Peckham, TL Smith, WR Moninger, JS Kenyon, and GS Manikin. 2016. "A North American Hourly Assimilation and Model Forecast Cycle: The Rapid Refresh." *Monthly Weather Review* 144(4): 1669–1694, https://doi.org/10.1175/MWR-D-15-0242.1

Clough, SA, and MJ Iacono. 1995. "Line-by-line calculation of atmospheric fluxes and cooling rates: 2. Application to carbon dioxide, ozone, methane, nitrous oxide and the halocarbons." *Journal of Geophysical Research – Atmospheres* 100(D8): 16519–16535, https://doi.org/10.1029/95JD01386

Clough, SA, MW Shephard, EJ Mlawer, JS Delamere, M Iacono, KE Cady-Pereira, S Boukabara, and PD Brown. 2005. "Atmospheric radiative transfer modeling: A summary of the AER codes." *Journal of Quantitative Spectroscopy and Radiative Transfer* 91(2): 233–244, https://doi.org/10.1016/j.jqsrt.2004.05.058

Coniglio, MC, GS Romine, DD Turner, and RD Torn. 2019. "Impacts of targeted AERI and Doppler lidar wind retrievals on short-term forecasts of the initiation and early evolution of thunderstorms." *Monthly Weather Review* 147(4): 1149–1170, https://doi.org/10.1175/MWR-D-0351.1

Feltz, WF, WL Smith, HB Howell, RO Knuteson, H Woolf, and HE Revercomb. 2003. "Near-Continuous Profiling of Temperature, Moisture, and Atmospheric Stability Using the Atmospheric Emitted Radiance Interferometer (AERI)." *Journal of Applied Meteorology* 42(5): 584–597, https://doi.org/10.1175/1520-0450(2003)042<0584:NPOTMA>2.0.CO;2

Grasmick, C, B Geerts, DD Turner, Z Wang, and TM Weckwerth. 2018. "The relation between nocturnal MCS evolution and its outflow boundaries in the stable boundary layer: An observational study of the 15 July 2015 MCS in PECAN." *Monthly Weather Review* 146(10): 3203–3226, https://doi.org/10.1175/MWR-D-18-0169.1

Haghi, KR, B Geerts, HG Chipilski, A Johnson, S Degelia, D Imy, DB Parsons, RD Adams-Selin, DD Turner, and X Wang. 2019. "Bore-ing into nocturnal convection." *Bulletin of the American Meteorological Society* 100(6): 1103–1121, https://doi.org/10.1175/BAMS-D-17-0250.1

Hu, J, N Yussouf, DD Turner, TA Jones, and X Wang. 2019. "Impact of ground-based remote sensing boundary layer observations on short-term probabilistic forecasts of a tornadic supercell event." *Weather and Forecasting* 34(5): 1453–1476, https://doi.org/10.1175/WAF-D-18-0200.1

Knuteson, RO, HE Revercomb, FA Best, NC Ciganovich, RG Dedecker, TP Dirkx, SC Ellington, WF Feltz, RK Garcia, HB Howell, WL Smith, JF Short, and DC Tobin. 2004. "Atmospheric Emitted Radiance Interferometer. Part 1: Instrument Design." *Journal of Atmospheric and Oceanic Technology* 21(12): 1763–1776, https://doi.org/10.1175/JTECH-1662.1

Knuteson, RO, HE Revercomb, FA Best, NC Ciganovich, RG Dedecker, TP Dirkx, SC Ellington, WF Feltz, RK Garcia, HB Howell, WL Smith, JF Short, and DC Tobin. 2004. "Atmospheric Emitted Radiance Interferometer. Part 2: Instrument Performance." *Journal of Atmospheric and Oceanic Technology* 21(12): 1777–1789, https://doi.org/10.1175/JTECH-1663.1

Lim, KS, LD Riihimaki, Y Shi, D Flynn, JM Kleiss, LK Berg, WI Gustafson, Y Zhang, and KL Johnson. 2019. "Long-term retrievals of cloud type and fair-weather shallow cumulus events at the ARM SGP site." *Journal of Atmospheric and Oceanic Technology* 36(10): 2031–2043, https://doi.org/10.1175/JTECH-D-18-0215.1

Mlawer, EJ, and DD Turner. 2016. "Spectral radiation measurements and analysis in the ARM program." *The Atmospheric Radiation Measurement Program: The First 20 Years*. American Meteorological Society, Meteorological Monograph 57: 14.1-14.17, https://doi.org/10.1175/AMSMONOGRAPHS-D-15-0027.1

Mlawer, EJ, DD Turner, SN Paine, L Palchetti, G Bianchini, VH Payne, KE Cady-Pereira, RL Pernak, MA Alvarado, D Gombos, JS Delamere, MG Mlynczak, and JC Mast. 2019. "Analysis of water vapor absorption in the far-infrared and sub-millimeter regions using surface radiometric measurements from extremely dry locations." *Journal of Geophysical Research – Atmospheres* 124(14): 8134–8160, https://doi.org/10.1029/2018JD029508

Payne, VH, EJ Mlawer, KE Cady-Pereira, and J-L Moncet. 2011. "Water vapor continuum absorption in the microwave." *IEEE Transactions on Geoscience and Remote Sensing* 49(6): 2194–2208, https://doi.org/10.1109/TGRS.2010.2091416

Rogers, CD. 2000. *Inverse Methods for Atmospheric Sounding: Theory and Practice*. World Scientific Publishing, Singapore.

Toms, BA, JM Tomaszewski, DD Turner, and SE Koch. 2017. "Analysis of a lower-tropospheric gravity wave train using direct and remote sensing measurement systems." *Monthly Weather Review* 145(7): 2791–2812, https://doi.org/10.1175/MWR-D-0216.1

Turner, DD. 2005. "Arctic mixed-phase cloud properties from AERI lidar observations: Algorithm and results from SHEBA." *Journal of Applied Meteorology* 44(4): 427–444, https://doi.org/10.1175/JAM2208.1

Turner, DD, RO Knuteson, HE Revercomb, C Lo, and RG Dedecker. 2006. "Noise reduction of Atmospheric Emitted Radiance Interferometer (AERI) observations using principal component analysis." *Journal of Atmospheric and Oceanic Technology* 23(9): 1223–1238, https://doi.org/10.1175/JTECH1906.1

Turner, DD. 2007. "Improved ground-based liquid water path retrievals using a combined infrared and microwave approach." *Journal of Geophysical Research* 112(D15): D15204, https://doi.org/10.1029/2007JD008530

Turner, DD, SA Clough, JC Liljegren, EE Clothiaux, K Cady-Pereira, and KL Gaustad. 2007. "Retrieving liquid water path and precipitable water vapor from Atmospheric Radiation Measurement (ARM) microwave radiometers." *IEEE Transactions on Geoscience and Remote Sensing* 45(11): 3680–3690, https://doi.org/10.1109/TGRS.2007.903703

Turner, DD, and U Löhnert. 2014. "Information content and uncertainties in thermodynamic profiles and liquid cloud properties retrieved from the ground-based Atmospheric Emitted Radiance Interferometer (AERI)." *Journal of Applied Meteorology and Climatology* 53(3): 752–771, https://doi.org/10.1175/JAMC-D-13-0126.1

Turner, DD, S Kneifel, and MP Cadeddu. 2016. "An improved liquid water absorption model at microwave frequencies for supercooled liquid water clouds." *Journal of Atmospheric and Oceanic Technology* 33(1): 33–44, https://doi.org/10.1175/JTECH-D-15-0074.1

Turner, DD, V Wulfmeyer, A Behrendt, TA Bonin, A Choukulkar, RK Newsom, WA Brewer, and DR Cook. 2018. "Response of the land-atmosphere system over north-central Oklahoma during the 2017 eclipse." *Geophysical Research Letters* 45(3): 1668–1675, https://doi.org/10.1002/2017GL076908

Turner, DD, and WG Blumberg. 2019. "Improvements to the AERIoe thermodynamic profile retrieval algorithm." *IEEE Journal of Selected Topics in Applied Earth Observations and Remote Sensing* 12(5): 1339–1354, https://doi.org/10.1109/JSTARS.2018.2874968

www.arm.gov

U.S. DEPARTMENT OF
ENERGY

Office of Science